Thermal rectification induced by Wenzel–Cassie wetting state transition on nano-structured solid–liquid interfaces

Haiyang Li(李海洋), Jun Wang(王军)†, and Guodong Xia(夏国栋)

MOE Key Laboratory of Enhanced Heat Transfer and Energy Conservation, Beijing Key Laboratory of Heat Transfer and Energy Conversion, Beijing University of Technology, Beijing 100124, *China*

(Received 1 October 2022; revised manuscript received 17 November 2022; accepted manuscript online 8 December 2022)

Thermal rectification refers to the phenomenon by which the magnitude of the heat flux in one direction is much larger than that in the opposite direction. In this study, we propose to implement the thermal rectification phenomenon in an asymmetric solid–liquid–solid sandwiched system with a nano-structured interface. By using the non-equilibrium molecular dynamics simulations, the thermal transport through the solid–liquid–solid system is examined, and the thermal rectification phenomenon can be observed. It is revealed that the thermal rectification effect can be attributed to the significant difference in the interfacial thermal resistance between Cassie and Wenzel states when reversing the temperature bias. In addition, effects of the liquid density, solid–liquid bonding strength and nanostructure size on the thermal rectification are examined. The findings may provide a new way for designs of certain thermal devices.

Keywords: thermal rectification, wetting transition, interfacial thermal resistance, solid–liquid interfaces

PACS: 44.90.+c, 61.30.Hn, 68.08.–p **DOI:** 10.1088/1674-1056/aca9c1

1. Introduction

Thermal rectification is a special heat transfer phenomenon by which the heat flux depends on the direction of the temperature gradient.[1,2] For a thermal rectifier, the magnitude of the heat flux in one direction is much larger than that in the opposite direction. Thermal rectification is of broad interest because it can be employed to control heat transfer and has potential applications in thermal computers,[3–5] recycling waste heat energy,[6,7] information processing,[8] and efficient use of the building energy.[9,10]

In the past decades, the thermal rectification phenomenon has been investigated in solid materials with asymmetric structures.[11–29] In 1936, the thermal rectification phenomenon has been reported in a system with copper/cuprous oxide interface, which is caused by the electron–phonon scattering at the interface.[11] Then, several thermal rectification mechanisms have been proposed, including the thermal potential barrier at the interface,[12] temperature-dependent interfacial thermal resistance or bulk thermal conductivity,[13,14] asymmetric nanostructures,[15] and electron transfer.[16] However, the thermal rectification effect is relatively weak. In a two-segment Frenkel–Kontorova lattice, a significant thermal rectification effect has been reported based on the temperature-dependent phonon band, and the ratio of the heat flux in the two opposite directions is larger than 100 times.[17,18] However, this ratio will decrease dramatically with increasing system size.[19] In experiments, thermal rectification effect has been observed in some low-dimensional nanomaterials. A solid-state thermal rectification phenomenon has been reported in carbon and boron nitride nanotubes with non-uniformly mass density, which is caused by the asymmetrical soliton transport.[20] The thermal rectification has also been experimentally studied in monolayer lateral heterojunctions, and it provides a platform for designing thermal rectifiers.[21,22] However, the primary drawbacks of thermal rectification in solid lattice systems are manufacturing difficulty.[23–29]

Recently, thermal rectification through solid–liquid (S–L) interfaces has been proposed, wherein the thermal rectification can be manipulated by varying the temperature and pressure of the system.[30–37] In Ref. [30], the thermal rectification phenomenon has been reported in an interfacial system with water and self-assembled monolayers silica, which is caused by the strong temperature dependence of the hydrogen bonds in water. Thermal rectification can also be achieved by varying the interfacial properties of the S–L interface,[31,32] applying an external force (electric or magnetic field) on the liquid molecules,[32] surface modifications with soft material,[31] different molecular mass between two artificial solid walls[33] or asymmetric molecular adsorption on the solid surface.[34–36] Although various thermal rectification models have been proposed, the thermal rectification effect in S–L systems is still limited, and the underlying mechanism for thermal rectification is still far from clarity.

The emergence of thermal rectification is generally attributed to some thermal transport properties which are temperature-dependent.[38–40] For solid–liquid interfacial thermal transport, the interfacial thermal resistance (ITR) plays an important role, which depends on the interfacial properties.[41–48] For a solid–liquid interface with nanostruc-

†Corresponding author. E-mail: jwang@bjut.edu.cn

© 2023 Chinese Physical Society and IOP Publishing Ltd

tured groves on the surface, its wettability state can be in the Cassie state and Wenzel state, depending on whether liquid molecules enter into the nanogrooves.[49–51] For the Cassie state, there are almost no fluid molecules inside the grooves; while for the Wenzel state, all grooves are filled with fluid molecules. The wetting transition between Cassie and Wenzel states is temperature-dependent and can cause sharp change in ITR. Thus, thermal rectification phenomenon may be realized in an S–L system by using the wetting transition between Cassie and Wenzel states.

In the present paper, a new thermal rectification mechanism is proposed in a heterogeneous nanostructured system by using the transition between Cassie and Wenzel wetting states. Based on the non-equilibrium molecular dynamics (NEMD) simulations, the thermal transport through a solid–liquid–solid system is investigated, and the thermal rectification phenomenon can be observed. Based on the calculation of the ITR, molecular density distribution, temperature distribution, the mechanism of thermal rectification is analyzed. In addition, we also examine the effect of the liquid density, solid–liquid bonding strength and nanostructure size on the thermal rectification.

2. Molecular dynamics simulation

The MD simulations were conducted by using the large-scale atomic/molecular massively parallel simulator (LAMMPS) packages.[52] Figure 1(a) shows a snapshot of the simulation system, which is composed of two outer solids (gold) and a fluid (argon) confined in the middle (a sandwiched system). The length of the system in y-direction is 8.2 nm, wherein the two solids have the same length of 1.0 nm, and the distance between the two outer solids is 6.2 nm. The cross-sectional area is 3.5 nm×5.0 nm in the x–z plane. The nanoribs are introduced on the left solid interface, wherein the height, width and spacing of the nanoribs structure are equal to 0.8 nm. The outermost atom layers in the y-direction are fixed (fixed boundary), and periodic boundary conditions are applied in x and z directions. The lattice constant of Au is $a = 0.406$ nm. Each bare surface consists of three layers face-centered cubic (FCC, $\{1\,1\,1\}$ plane) Au-based solid. The number of fluid molecules of argon is $N_{\mathrm{F}} = 1260$.

The interactions between fluid molecules is described by the Lennard–Jones (LJ) potential, $U_{ij} = 4\varepsilon[(\sigma/r_{ij})^{12} - (\sigma/r_{ij})^{6}]$, where r_{ij} is the distance between atoms i and j, σ and ε are the collision diameter and the potential well depth. The LJ potential parameters of argon are summarized in Table 1.[53] The interactions between solid–solid and solid–liquid atoms are modeled by Morse potential

$$U_{ij} = D\left[\mathrm{e}^{-2\alpha(r_{ij}-r_0)} - 2\,\mathrm{e}^{-\alpha(r_{ij}-r_0)}\right], \tag{1}$$

where D is the potential well depth, α and r_0 are the well width and collision diameter for the Morse potential, respectively. The atomic interaction parameters are listed in Table 1, in which superscripts s and l represent the solid and liquid molecules.[54,55] A coupling parameter c is introduced to describe the S–L interfacial coupling strength, $D^{\mathrm{sl}} = cD^{\mathrm{sl}}$. In the present paper, the coupling parameter c is set to be 0.05, at which the S–L surface is hydrophobic and the contact angle is about 140°.

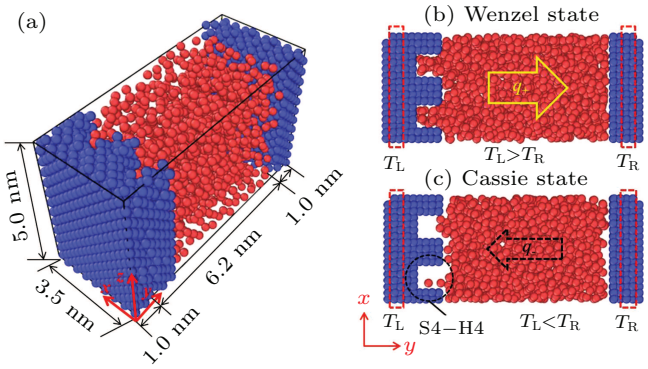


Fig. 1. (a) Snapshot of the thermal rectification simulation system; (b) q_+ for the high thermal transport of Wenzel state; (c) q_- for the low thermal transport of Cassie state.

Table 1. Potential parameters.

σ (nm)	ε (eV)	D^{ss} (eV)	α^{ss} (nm^{-1})
0.3405	0.10324	0.4905	0.166136
$r_{\mathrm{o}}^{\mathrm{ss}}$ (nm)	D^{sl} (eV)	α^{sl} (nm^{-1})	$r_{\mathrm{o}}^{\mathrm{sl}}$ (nm)
0.299032	0.01395	0.13781	0.41024

The velocity-verlet algorithm is applied to integrate the equations of motion for the atoms. The time-step $\Delta t = 1$ fs. For all inter-molecular interactions, the cut-off distance is set as 1.0 nm. The whole system is first equilibrated at temperature T for 2 ns by using the Langevin thermostat (NVT ensemble). Then, the thermal thermostat is removed and the system is relaxed at the NVE ensemble for 1 ns. After that, the Langevin thermostats with temperatures T_{L} and T_{R} are applied to the three layers adjacent to the leftmost and rightmost layers, respectively. After running for 20 ns, the non-equilibrium steady state is established. The following 10 ns is used for information collection. The heat flux is calculated by

$$q = \Delta E/(\Delta t \cdot A), \tag{2}$$

where ΔE is the average energy removed in the cold thermostat and added in the hot thermostat, Δt is the time step, A is the cross section area in the x–z plane. To minimize statistical error, at least five independent simulations with different initial conditions (atoms with different initial velocities which follow the same Maxwell velocity distribution) are conducted and the averaged value is considered as the final result.

In our simulations, the temperature T_0 is set as 150 K, and the temperatures of the left and right thermal thermostats are

set as $T_{\rm L} = T_0(1+\Delta)$ and $T_{\rm R} = T_0(1-\Delta)$, respectively. Here, Δ is the dimensionless temperature difference. For $\Delta > 0$, the heat transfer is from left to right, and the heat flux is denoted by q_+ (L–R mode). For $\Delta < 0$, the corresponding heat flux is q_- (R–L mode).

3. Results and discussion

3.1. Thermal rectification simulation results

Figure 2(a) plots the heat flux versus the dimensionless temperature difference Δ. It is clearly seen that the magnitude of the heat flux for the L–R mode is always higher than that in the opposite direction (R–L mode). In the case of the $\Delta > 0$, q_+ increases linearly with Δ. In the case of $\Delta < 0$, the heat flux increases with $|\Delta|$, then decreases for larger $|\Delta|$, i.e., negative differential thermal resistance can be observed in this system.[56–58] To describe the thermal rectification effect, the thermal rectification factor $\gamma = |q_+|/|q_-|$ is introduced, where $|q_+|$ and $|q_-|$ are heat fluxes in the favorable and unfavorable directions, respectively. As shown in Fig. 2(b), the thermal rectification can be implemented in the whole temperature range, and the thermal rectification factor increases significantly with $|\Delta|$ (from $\gamma = 1.2$ at $|\Delta| = 0.05$ to $\gamma = 13.7$ at $|\Delta| = 0.8$).

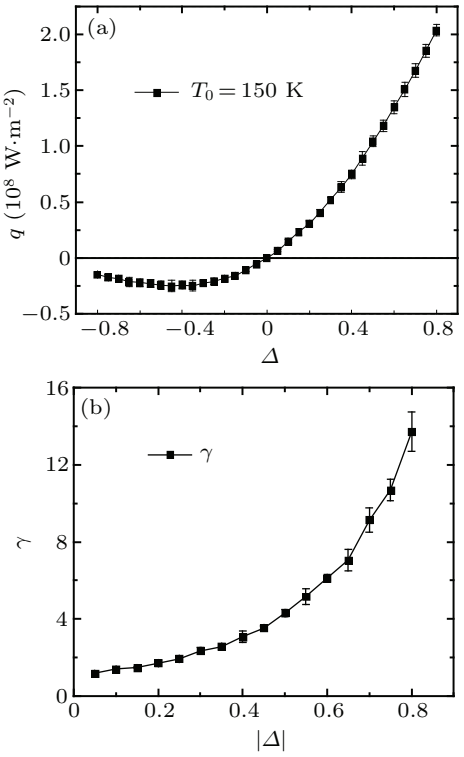


Fig. 2. (a) Heat flux q and (b) thermal rectification factor γ versus dimensionless temperature difference Δ for $T_0 = 150$ K.

3.2. Mechanism for thermal rectification

To study the mechanism of thermal rectification in the present sandwiched system, the thermal resistance of the system is calculated. Figure 3 plots the thermal resistances contributed by the left S–L interface ($R_{\rm int,L}$), the confined liquid in the system ($R_{\rm liq,F}$) and the right S–L interface ($R_{\rm int,R}$). The thermal resistance is calculated by using $R = \Delta T/q$. Here, the liquid temperature profile is lengthened to the interface, and the temperature difference ΔT is defined as the difference between the solid temperature and the extended liquid temperature.[44] The thermal resistance of the solid can be neglected owing to its high thermal conductivity with respect to the thermal conductivity of a fluid. As shown in Fig. 3, the largest thermal resistance contribution is from the flat surface (right surface), followed by the ITR of the nanostructured surface. $R_{\rm liq,F}$ can be ignored compared to $R_{\rm int,L}$ and $R_{\rm int,R}$. Thus, the ITR dominates the thermal transport through the system. In the case of $\Delta < 0$, both the ITRs of the flat and nanostructured surfaces increase with $|\Delta|$. When reversing the temperature bias ($\Delta > 0$), the ITRs of the flat and nano-structured surfaces are relatively small, and decrease gradually with $|\Delta|$. As a result, the thermal rectification phenomenon can be observed in the present system, and the thermal rectification factor increases with $|\Delta|$.

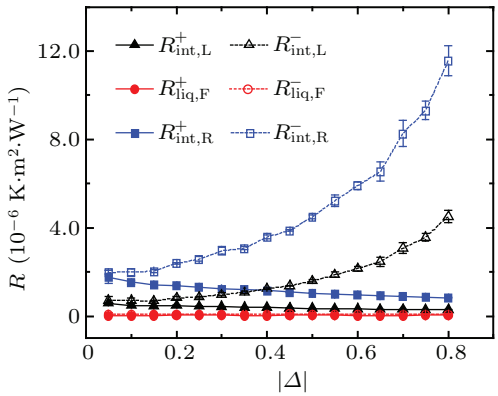


Fig. 3. The left ITR, $R_{\rm int,L}$, the thermal resistance of the bulk liquid, $R_{\rm liq,F}$, and the right ITR, $R_{\rm int,R}$, versus $|\Delta|$. Here + and − represent the L–R and R–L modes, respectively.

The two-dimensional density distributions of fluid molecules for $\Delta < 0$ and $\Delta > 0$ are illustrated in Fig. 4. It is shown that the density of the fluid molecules inside the nanogrooves for $\Delta = -0.2$ is much less than that for $\Delta = 0.2$, as shown in Figs. 4(a) and 4(d). For $\Delta > 0$, the density of fluid molecules in the nanogrooves increases with $|\Delta|$. On the other hand, for $\Delta < 0$, the fluid molecular density in the nanogrooves decreases with $|\Delta|$, and there are almost no liquid molecules for $\Delta = -0.8$. For higher $|\Delta|$, the nano-structured surface is close to the Wenzel state in the case of $\Delta > 0$, while in the case of $\Delta < 0$, it is in Cassie wetting state. Therefore, the transition between Wenzel and Cassie wetting states can be observed when reversing the temperature bias, and a significant change in the ITR on the nano-structured surface can be expected.

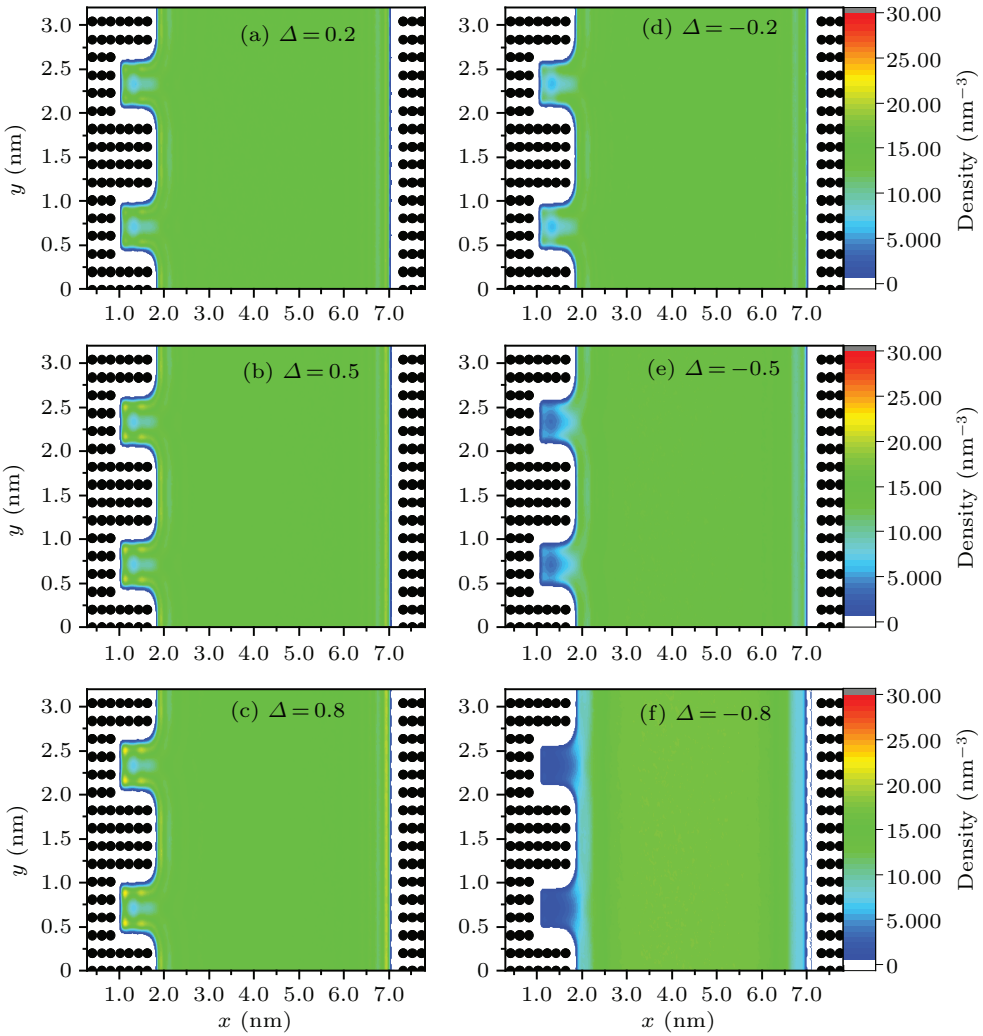


Fig. 4. Two-dimensional density distribution of fluid molecules at various dimensionless temperature differences Δ: (a)–(c) $\Delta > 0$; (d)–(f) $\Delta < 0$.

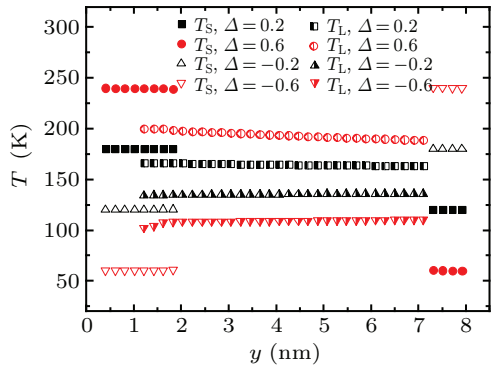


Fig. 5. The temperature profile of the system along the y-direction for $|\Delta| = 0.2$ and $|\Delta| = 0.6$.

Figure 5 shows the temperature profiles of the system along the y direction for $|\Delta| = 0.2$ and $|\Delta| = 0.6$. The temperature jump in the liquid region is much smaller than that in the S–L interface due to the low thermal resistance of the bulk liquid, $R_{\text{liq,F}}$. Compared with the left solid–liquid interface (nano-structured surface), the right interface (flat surface) has a higher temperature jump. This is because the ITR on the flat surface is usually higher than that on the nano-structured surface.[44] For $\Delta > 0$, the temperature of the bulk liquid is close to the high temperature ($T_L > T_R$), which results in a high liquid pressure, as shown in Fig. 6 (wherein the average temperature T and pressure P of the bulk liquid are plotted). In this case, the fluid molecules can permeate into the nano-grooves (i.e., Wenzel state). On the right S–L interface, the fluid molecules are adsorbed tightly on the solid surface owing to the high liquid pressure (see Fig. 4) and a well thermal contact can be expected. Figure 7 plots the ITRs of flat and nano-structured surfaces as a function of the system pressure. It can be seen that the thermal resistance decreases with the system pressure in the form of $R \propto P^{\alpha}$ for both flat and nano surfaces.[41,42] The power-law exponents of the linear fits are $\alpha_1 = 0.94$ and $\alpha_2 = 1.02$ for the flat and nano-structured surfaces, respectively. Therefore, for $\Delta > 0$, the ITRs on both the left and right interfaces are relatively low and gradually decreases with increasing Δ, as shown in Fig. 3. For $\Delta < 0$, the liquid is close to the low temperature ($T_L < T_R$), then the liquid pressure is relatively low (see Fig. 6) and the fluid molecules cannot permeate into the nano-grooves (Cassie state). Meanwhile, the thermal contact is weak on the right surface (see Fig. 4). Thus, in the case of $\Delta < 0$, high ITRs on the flat and

nano-structured interfaces are expected (see Fig. 7), and the thermal transport through the system can be suppressed. As a result, with increasing $|\Delta|$, the thermal transport in the L–R mode is enhanced while the heat transfer in the opposite direction is suppressed. Then, the thermal rectification factor increases with $|\Delta|$.

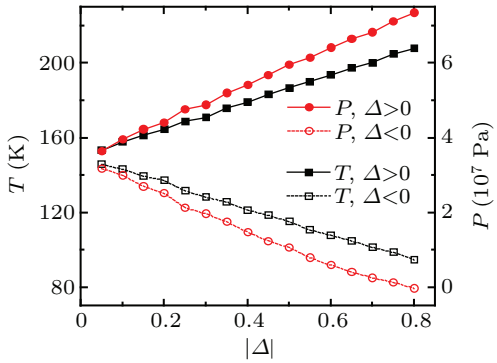


Fig. 6. The averaged temperature T and pressure P of the bulk liquid profiles for the L–R and R–L modes versus $|\Delta|$.

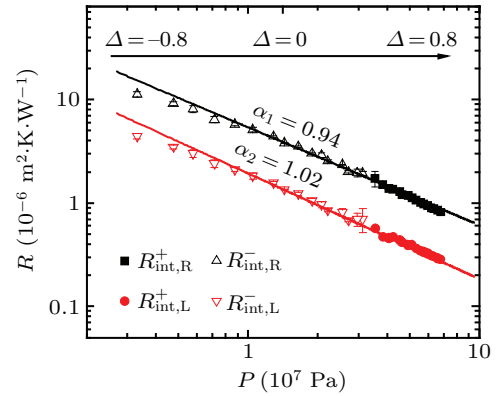


Fig. 7. Interfacial thermal resistances of flat and nanostructured surfaces versus pressure P of the liquid.

3.3. Thermal rectification effect with varying interfacial coupling strength, liquid density and nanostructured surface

The S–L interaction strength, the liquid density and nanostructure size are important parameters which can affect the thermal rectification. Here, we set $\Delta = 0.6$, $T_0 = 150$ K, $N_F = 1260$. To study the effect of S–L interfacial coupling strength on the thermal rectification, the coupling parameter c is varied from 0.05 to 0.5, which corresponds to surface wettability transition from hydrophobic to hydrophilic. The variations of heat flux and thermal rectification with parameter c are shown in Fig. 8. The heat flux through the sandwiched system in both directions increases significantly with the parameter c. Here $|q_+|$ is always larger than $|q_-|$. However, the thermal rectification factor decreases with increasing c. The state transition between Cassie and Wenzel states is related to the wettability of the interface. For the hydrophilic interfaces, the fluid molecules can easily flow into nano-grooves owing to the strong interfacial adsorption. Therefore, the state transition between Cassie and Wenzel states when reversing the temperature bias is not significant for large c, which results in a smaller difference in ITRs and lower thermal rectification factor.[59]

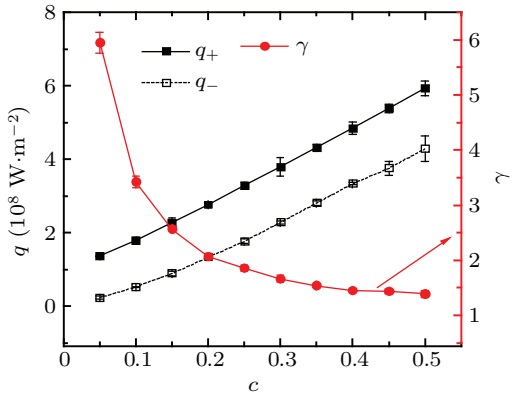


Fig. 8. Heat flux q and thermal rectification factor γ as a function of the solid–liquid interfacial coupling parameter c.

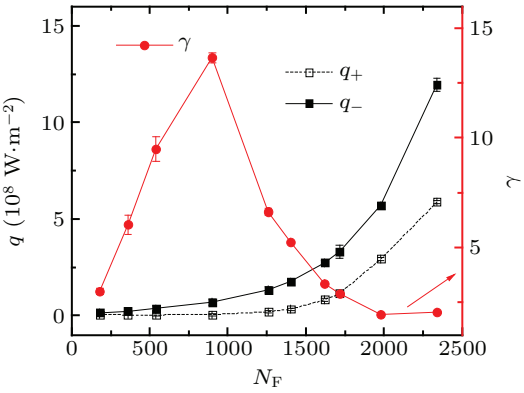


Fig. 9. Heat flux q and the thermal rectification factor γ versus the number of fluid molecules N_F for $|\Delta| = 0.6$ and $c = 0.05$.

The pressure of the system is mainly determined by the number of fluid molecules, which is another important factor affecting thermal rectification. Figure 9 plots the heat flux q through the system and thermal rectification factor γ versus the number of fluid molecules (N_F). Here, $|\Delta| = 0.6$ and $c = 0.05$. It can be seen that both $|q_+|$ and $|q_-|$ increase with N_F. Thermal rectification factor γ increases with N_F for small N_F, and decreases after reaching a maximal value at about $N_F = 900$. In the present paper, the thermal rectification is caused by surface wettability transition between Wenzel and Cassie states. The Cassie–Wenzel wetting transition is determined by a critical pressure p_0, where p_0 is the system pressure.[49,50] In this system ($c = 0.05$), the critical pressure p_0 is about 8 MPa. At small N_F, the pressures of both L–R and R–L modes are smaller than critical pressure p_0 (such as $N_F = 360$, the pressures of both L–R and R–L modes are about 3.2 MPa and 0.43 MPa). On the contrary, the pressures of both modes are greater than critical pressure p_0 at the larger N_F (such as $N_F = 1620$, the pressures of both L–R and R–L modes are about 40.6 MPa and 13.1 MPa). In both cases, there is no surface wettability transition when reversing the temperature gradient, which leads to the low thermal rectification factor.

Therefore, there is an optimal number of fluid molecules in the system.

In our MD simulation, varying nano-rib structure size is also considered. Figure 10 plots the influence of nanostructure size on the thermal rectification effect. The nanostructure is denoted by S*m*–H*n*, wherein S*m* denotes the width and gap of the nano-rib with *m* layers of solid atoms, and H*n* denotes nano-rib height with *n* layers of solid atoms, respectively. The structure shown in Fig. 1 corresponds to S4–H4. It is found that the thermal rectification ratio can be enhanced with the decrease of the width and gap of the nanoribs, as shown in Fig. 10(a). This is because the solid–liquid interface contact area is increased, which in turn amplifies the liquid pressure difference between Wenzel and Cassie states and enhances the thermal rectification factor. For a fixed gas size, the solid–liquid interface contact area is reduced for lower nanoribs, then the effect of the Wenzel and Cassie states transition is weak. For the higher nano-ribs, the volume of nano-gap decreases and the liquid density increases. Then, according to Fig. 9, the thermal rectification effect can be weaken. Thus, there is an optimal nano-rib (S4–H4) to achieve the maximum thermal rectification efficiency with varying nano-rib height, as shown in Fig. 10(b).

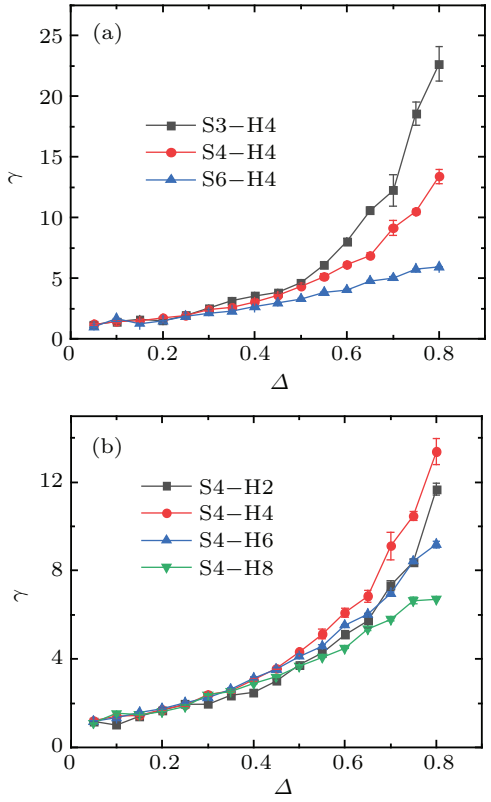


Fig. 10. Thermal rectification factor γ versus the temperature different Δ with (a) varying nano-rib width and gap size and (b) height size.

4. Conclusions

In summary, we have examined the asymmetric thermal transport through a solid–liquid–solid sandwiched system with a nano-structured surface, based on non-equilibrium molecular dynamic simulations. It is demonstrated that thermal rectification can be implemented and the thermal rectification factor increases with increasing dimensionless temperature difference. The wettability transition between Wenzel and Cassie states when reversing the temperature bias is responsible for the thermal rectification effect, which leads to a significant difference in the interfacial thermal resistance and in turn results in the thermal rectification phenomenon. Further results show that the solid–liquid bonding strength and liquid density have a significant impact on the thermal rectification factors. The thermal rectification factor gradually decreases with the increase of the solid–liquid bond strength. With varying liquid density, there is an optimal fluid molecular number, which results in the maximum thermal rectification factor. The thermal rectification model proposed in this paper may provide a new way for designs of thermal management systems.

Acknowledgements

Project supported by the National Natural Science Foundation of China (Grant No. 51976002), and the Beijing Nova Program of Science and Technology (Grant No. Z191100001119033).

References

[1] Roberts N A and Walker D G 2011 *Int. J. Therm. Sci.* **50** 648
[2] Wehmeyer G, Yabuki T, Monachon C, Wu J and Dames C 2017 *Appl. Phys. Rev.* **4** 041304
[3] Li N, Ren J, Wang L, Zhang G, Hänggi P and Li B W 2012 *Rev. Mod. Phys.* **84** 1045
[4] Wong M Y, Tso C Y, Ho T C and Lee H H 2021 *Int. J. Heat Mass Transfer* **164** 120607
[5] Wang L and Li B W 2007 *Phys. Rev. Lett.* **99** 177208
[6] Kuo M and Chang Y 2010 *Phys. Rev. B* **81** 205321
[7] Roberts N A and Walker D G 2011 *J. Heat Transfer* **133** 092401
[8] Paolucci F, Marchegiani G, Strambini E and Giazotto F 2018 *Phys. Rev. Appl.* **10** 024003
[9] Varga S, Oliveira A C and Afonso C F 2002 *Energy Build.* **34** 227
[10] Henry A, Prasher R and Majumdar A 2020 *Nat. Energy* **5** 635
[11] Starr C 1936 *Physics* **7** 15
[12] Rogers G F C 1961 *Int. J. Heat Mass Transfer* **2** 150
[13] Zhao J N, Wei D, Shang X C and Liu D H 2022 *Int. J. Heat Mass Transfer* **194** 123024
[14] Wang J, Shao C R, Li H Y and Xia G D 2022 *Int. J. Heat Mass Transfer* **188** 122627
[15] Yang N, Zhang G and Li B W 2009 *Appl. Phys. Lett.* **95** 33107
[16] Craven G T, He D H and Nitzan A 2018 *Phys. Rev. Lett.* **121** 247704
[17] Terraneo M, Peyrard M and Casati G 2002 *Phys. Rev. Lett.* **88** 094302
[18] Li B W, Wang L and Casati G 2004 *Phys. Rev. Lett.* **93** 184301
[19] Hu B B, Yang L and Zhang Y 2006 *Phys. Rev. Lett.* **97** 124302
[20] Chang C W, Okawa D, Majumder A and Zettl A 2006 *Science* **314** 1121
[21] Zhang Y F, Lv Q, Wang H D, Zhao S Y, Xiong Q H, Lv R T and Zhang X 2022 *Science* **378** 169
[22] Wang H, Hu S, Takahashi K, Zhang X, Takamatsu H and Chen J 2017 *Nat. Commun.* **8** 1
[23] Yuan K P, Sun M M, Wang Z L and Tang D W 2015 *Int. J. Therm. Sci.* **98** 24
[24] Feng F and Liang X 2017 *J. Heat Transfer* **139** 052402
[25] He D H, Thingna J and Cao J S 2018 *Phys. Rev. B* **97** 195437
[26] Zhan S Q, Huang W Q and Huang G F 2014 *Chin. Phys. B* **23** 114401
[27] Zhang Z W, Ouyang Y L, Chen J and Sebastian V 2020 *Chin. Phys. B* **29** 124402

[28] Zhou H and Zhang G 2018 *Chin. Phys. B* **27** 034401
[29] Wang Z, Zhang D M and Ren J 2019 *Acta Phys. Sin.* **68** 220302 (in Chinese)
[30] Hu M, Goicochea J V, Michel B and Poulikakos D 2009 *Appl. Phys. Lett.* **95** 151903
[31] Murad S and Puri I K 2014 *Appl. Phys. Lett.* **104** 211601
[32] Murad S and Puri I K 2012 *J. Chem. Phys.* **137** 3714
[33] Feng F and Liang X G 2015 *Int. J. Thermophys.* **36** 1519
[34] Avanessian T and Hwang G 2018 *Int. J. Heat Mass Transfer* **124** 201
[35] Avanessian T and Hwang G 2016 *J. Appl. Phys.* **120** 165306
[36] Li F, Li H Y, Wang J and Xia G D 2022 *J. Therm. Sci.* **31** 10
[37] Meng Z, Gulfam R and Zhang P 2021 *Int. J. Therm. Sci.* **164** 106856
[38] Hong Y, Zhang J and Zeng X C 2018 *Chin. Phys. B* **27** 036501
[39] Li Y Y, Li N B, Tirnakli U, Li B W and Tsallis C 2017 *Europhys. Lett.* **117** 60004
[40] Peng G L, Xu Z W, Ji J J, Sun S S and Yang N 2022 *Appl. Thermal Eng.* **213** 118664
[41] Pham A, Barisik M and Kim B H 2013 *J. Chem. Phys.* **139** 244702
[42] Han H, Mérabia S and Müller-Plathe F 2017 *J. Phys. Chem. Lett.* **8** 1946
[43] Hu M, Goicochea J V, Michel B and Poulikakos D 2009 *Nano Lett.* **10** 279
[44] Lin T, Li J, Quan X and Cheng P 2018 *Int. Commun. Heat Mass Transfer* **97** 118
[45] Song G and Chen M 2013 *Mol. Phys.* **111** 903
[46] Cao Q, Cui Z and Shao W 2020 *Langmuir* **36** 2802
[47] Harikrishna H, Ducker W A and Huxtable S T 2013 *Appl. Phys. Lett.* **102** 251606
[48] Li H Y, Wang J and Xia G D 2022 *J. Therm. Sci.* **31** 13
[49] Zheng Q S, Yu Y and Zhao Z H 2005 *Langmuir* **21** 12207
[50] Cai T M, Jia Z H, Yang H N and Wang G 2016 *Colloid Polym. Sci.* **294** 833
[51] Yin L, Lin P and Qi X 2014 *Chin. Phys. Lett.* **31** 114401
[52] Plimpton S 1995 *J. Comput. Phys.* **117** 1
[53] Hippler H 1983 *J. Chem. Phys.* **78** 6709
[54] Pamuk H Ö and Halicioğlu T 1976 *Phys. Status Solidi A* **37** 695
[55] Grenier R, To Q D, Lara-Castells M P D and Leonard C 2015 *J. Phys. Chem. A* **119** 6897
[56] Li F, Wang J, Xia G D and Li Z G 2019 *Nanoscale* **11** 13051
[57] Li F, Wang J and Xia G D 2020 *J. Phys. Chem. C* **124** 92
[58] Chan H K, He D H and Hu B 2014 *Phys. Rev. E* **89** 052126
[59] Surblys D, Kawagoe Y, Shibahara M and Ohara T 2019 *J. Chem. Phys.* **150** 114705